Fluid Phase Equilibria 314 (2012) 1–6

Contents lists available at SciVerse ScienceDirect

Fluid Phase Equilibria

journal homepage: www.elsevier.com/locate/fluid

Prediction of the mutual solubility of water and dipropylene glycol dimethyl ether using molecular dynamics simulation

Tao Cheng, Feng Li, Jianxing Dai, Huai Sun*

School of Chemistry and Chemical Engineering, Shanghai Jiao Tong University, China

ARTICLE INFO

Article history:
Received 23 March 2011
Received in revised form
20 September 2011
Accepted 14 October 2011
Available online 20 October 2011

Keywords:
Mutual solubility
Molecular dynamics
Gibbs free energy
Double tangent method

ABSTRACT

Molecular dynamics (MD) simulations were applied to investigate the liquid–liquid equilibria of water and dipropylene glycol dimethyl ether (DMM) based on all-atom OPLS force fields and simple point charge (SPC) water model. The default combining rules (geometric means) for describing interactions between water and ether molecules were modified by fitting hydration free energies of dimethyl ether and diethyl ether. The difference of Gibbs free energies (ΔG) was calculated using the thermodynamic integration (TI) method. Extensive simulations were carried out in order to reach high precision in the predicted free energies. The average uncertainties in calculated ΔG are 0.8 kJ/mol for DMM and 0.3 kJ/mol for water. From the calculated ΔG^{mix}, the mutual solubility of the binary mixture was predicted using the double tangent method at four temperatures ranging from 283 K to 353 K and 1 atm.

1. Introduction

Using molecular simulation methods to predict liquid–liquid-equilibrium (LLE) remains to be a great challenge. Several simulation methods have been developed for predicting phase equilibrium. These include Gibbs ensemble Monte Carlo [1], isomolar semigrand ensemble molecular dynamics [2], multiple-histogram reweighting [3], Gibbs–Duhem integration (GDI) [4], the N–P–T plus test particle method [5], to name a few. In principle, most of these methods can be applied to predict LLE. However, a general problem for predicting LLE properties is about the efficiency of simulation. As a result, reports concerning the prediction of LLE from direct MD or MC simulation are scarce. Morrow and Maginn [2] developed an extended system molecular dynamics method for an isomolar semigrand ensemble method to investigate LLE for two Lennard–Jones mixtures. Instead of particle insertions and deletions, they employed a gradual and dynamical trial particle transformations, which is more efficient in condense phase simulation. Kristóf et al. [6] proposed an extrapolation scheme to determine the VLE and LLE equilibrium curves of binary mixtures basing on data obtained from GEMC simulation. This scheme was successfully applied in binary Lennard–Jones mixtures. However, to our best knowledge, no successful perditions have been reported for real systems.

Greater challenge is also related to the capability of a force field in describing interactions for unlike molecules in mixtures. Classical force fields do not represent intermolecular polarization dynamically, leading to poor predictions even for the simplest properties such as heat of mixing [7]. Recently, notable progresses have been made in developing polarizable force fields. Ponder et al. [8] developed a polarizable force field, AMOEBA, which showed significant improvement over fixed charge models for thermodynamic observables, such as hydration free energy. However, for polarizable force field, parameterization is difficult and parameters are not generally available. In addition, the much higher requirement for computational resources by using the polarizable force fields worsens the efficiency problem. At present, using classical force fields, optimized to include the polarization in an average manner, is a more promising approach to study the mixtures. Schnabel et al. [9] adjusted the unlike dispersive interaction according to experimental binary vapor–liquid equilibrium data, which greatly improved the accuracy of mixture model without scarifying computation efficiency.

In this work, we attempt to predict mutual solubility of water and dipropylene glycol dimethyl ether (DMM) that exhibits an "inverse solubility" relationship with water by directly calculating the Gibbs free energy change of mixing (ΔG^{mix}). Realizing the challenges are mainly in force field quality and simulation efficiency, we modified the combining rules to effectively include the polarization effect and extended the simulations to the limit that our computational resources can provide. The modification of force field was validated by calculating hydration free energies of dimethyl ether and diethyl ether. The average uncertainties in predicted free energy (ΔG) changes are less than 0.8 kJ/mol. Unfortunately, this unprecedented low uncertainty is still too large in comparison with the absolute values of ΔG^{mix}, which impairs our ability to predict

* Corresponding author. Tel.: +86 21 5474 8987 601; fax: +86 21 5474 1297.
E-mail address: huaisun@sjtu.edu.cn (H. Sun).

0378-3812/$ – see front matter © 2011 Elsevier B.V. All rights reserved.
doi:10.1016/j.fluid.2011.10.013

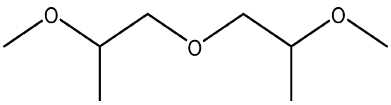

Fig. 1. Molecular structure of DMM.

the mutual solubility accurately. However, the techniques used in this work have been shown promising and the efficiency problem can be eventually solved with increasing computer power.

2. Model and methods

One of the three possible isomers of DMM (see Fig. 1) was considered in this work. The simulated mixtures of DMM and water in terms of molar percentage and weight percentage are listed in Table 1.

The SPC model [10] was used for water, the OPLS all-atom force field [11] was used for DMM. The potential energy function for both models can be described as following:

$$E = \sum_{bonds} K_r(r - r_{eq})^2 + \sum_{angles} K_\theta(\theta - \theta_{eq})^2 + \sum_{dihedral} \left\{ \frac{V_1}{2}[1 + \cos(\phi + f1)] + \frac{V_2}{2}[1 - \cos(2\phi + f2)] + \frac{V_3}{2}[1 + \cos(3\phi + f3)] \right\} + \sum_{nonbond} \left\{ 4\varepsilon_{ij} \left[\left(\frac{\delta_{ij}}{R_{ij}} \right)^{12} - \left(\frac{\delta_{ij}}{R_{ij}} \right)^{6} \right] + \frac{q_i q_j e^2}{r_{ij}} \right\} \quad (1)$$

Unlike-atom interactions are computed using geometric mean combining rules

$$\delta_{ij} = \sqrt{\delta_{ii}\delta_{jj}} \quad (2)$$

$$\varepsilon_{ij} = \sqrt{\varepsilon_{ii}\varepsilon_{jj}} \quad (3)$$

A scaling factor of 1/2 is used for the 1–4 intramolecular electrostatic interaction and 1–4 van der Waals interaction.

Molecular dynamics simulations were carried out using Gromacs 4.0.3 [12]. The weak coupling technique velocity rescaling [13] was used to modulate the temperature with relaxation time of 0.2 ps. Isotropic pressure control of Parrinello–Rahman [14] was used with relaxation times of 0.4 ps. All of the X–H bonds were constrained by LINCS [15] method with a tolerance of 0.0001 and LINCS order 4.0. A 2 fs time step for integration of the equations of motion was chosen. A cutoff radius of 1.2 nm was employed to calculation the van der Waals interaction in free energy calculation and 1.5 nm for surface tension calculation. A long-range dispersion correction was added to both energy and pressure. Long-range electrostatics was handled using the particle mesh Ewald technique [16] with a real-space cutoff of 1.2 nm for free energy calculation and 1.5 nm for surface tension calculation with a grid resolution of 0.12 nm. The nonbond list was updated every 5 steps.

Table 1
Mixtures with different compositions calculated in this work.

DMM		No. of molecules	
wt%	mol%	DMM	Water
0	0	0	1000
10	1	20	1620
35	6	50	835
69	20	100	400
80	31	100	223
86	40	100	150
90	50	100	100
93	60	100	68
95	68	100	47
98	84	105	20
99	90	105	12
100	100	100	0

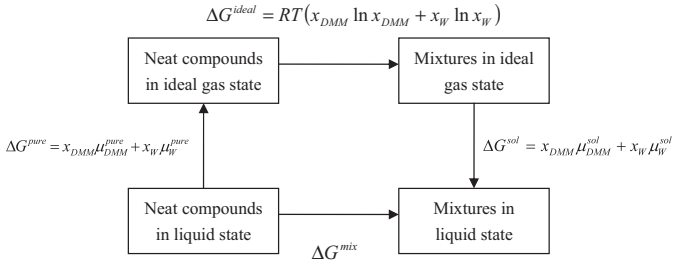

Fig. 2. Thermodynamic cycle along which the two neat liquid compounds are brought to their liquid mixture in the calculations.

The Gibbs free energy change of mixing ΔG^{mix} was calculated using NPT simulations on a thermodynamic cycle [17] as shown in Fig. 2. For a selected composition (fixed molar percentage x_{DMM} and x_W), the Gibbs free energy change of mixing ΔG^{mix} is equivalent to three contributions: (i) Gibbs free energy change for bringing molecules from their pure liquid state to ideal-gas state (ΔG^{pure}); (ii) ideal Gibbs free energy change of mixing (entropy of mixing) of the two compounds in ideal gas state (ΔG^{ideal}); and (iii) Gibbs free energy change for bringing molecules from their mixed ideal gas state to liquid state (ΔG^{sol}). Overall, the ΔG^{mix} is the sum of the three Gibbs free energy changes:

$$\Delta G^{mix} = \Delta G^{sol} - \Delta G^{pure} + \Delta G^{ideal} \quad (4)$$

ΔG^{ideal} was calculated analytically:

$$\Delta G^{ideal} = RT(x_{DMM} \ln x_{DMM} + x_W \ln x_W) \quad (5)$$

ΔG^{pure} and ΔG^{sol} were calculated from chemical potentials of the compounds.

$$\Delta G^{pure} = x_{DMM}\mu^{pure}_{DMM} + x_W\mu^{pure}_W \quad (6)$$

$$\Delta G^{sol} = x_{DMM}\mu^{sol}_{DMM} + x_W\mu^{sol}_W \quad (7)$$

The chemical potentials in Eqs. (6) and (7) were calculated using the thermodynamic integration (TI) method [18] implemented in GROMACS. For mixtures, a simulation box was prepared by randomly mixing the molecules at each composition. The chemical potential for a component was calculated by randomly selecting a molecule in the type and gradually taking it from its initial state ($\lambda = 0$) to its end state ($\lambda = 1$). At the initial state the intermolecular potential energy of the molecule is in full strength and at the end state the intermolecular potential energy is set to zero. The transition was done by applying a coupling parameter λ in a series of MD simulations. At constant temperature and pressure the Gibbs free energy change, the chemical potential, of the selected compound is calculated as following:

$$\mu = \Delta G = \int_{\lambda=0}^{\lambda=1} \left\langle \frac{\partial H}{\partial \lambda} \right\rangle_\lambda d\lambda = \int_{\lambda=0}^{\lambda=1} \left\langle \frac{\partial V}{\partial \lambda} \right\rangle_\lambda d\lambda \quad (8)$$

The last equation is without kinetic energy term, because the coupling parameter is only applied to the potential energy term. The bracket in Eq. (8) means ensemble average at given value of the coupling parameters.

Eq. (8) can be used to calculate hydration free energy (ΔG_{hyd}) which is the chemical potential of the solute molecule in infinite amount of water under constant temperature and pressure. The simulation was done by placing one solute molecule in a box of water, and using the TI method to decouple the solute molecule from the solution.

The accuracy of free energy calculation depends on a number of factors. The number of decoupling points is one of the critical parameters. After an initial study, a scheme with 26 λ-points and an interval of 0.04 between adjacent points was used in this work. The soft-core potential [19] was used to remove singularities associated with the intermolecular potential energies (Lennard–Jones and Coulomb) when molecule disappears (λ close to 1). For a pair interaction potential $V(r)$, the soft-core potential $V_{sc}(r)$ is given as a combination of the potentials at state A ($\lambda = 0$) and state B ($\lambda = 1$):

$$V_{sc}(r) = (1-\lambda)V^A(r_A) + \lambda V^B(r_B) \quad (9)$$

$$r_A = (\alpha\delta_A^6\lambda^p + r^6)^{1/6} \quad (10)$$

$$r_B = (\alpha\delta_B^6(1-\lambda)^p + r^6)^{1/6} \quad (11)$$

where α and p are adjustable parameters which determine the shape of the correction curve. We optimized both parameters aiming for smooth $\langle \delta V/\delta\lambda \rangle$ curves and obtained 2.0 and 0.5 for p and α respectively. The Van der Waals radius δ_A and δ_B were set to their normal values by default but fixed to 0.3 nm when the atom–atom distances were less than 0.3 nm.

From Eq. (4), the excess Gibbs free energy change of mixing (ΔG^{excess}) may be defined as:

$$\Delta G^{excess} = \Delta G^{sol} - \Delta G^{pure} \quad (12)$$

Both terms in the right hand of Eq. (12) were obtained using the TI method and the data are associated with large uncertainties. In order to get a smooth ΔG^{excess} curve in the full range of composition, we fitted the simulated ΔG^{excess} points to Redlich–Kister equation: [20]

$$\Delta G^{excess} = RTx_{DMM}x_W[A + B(x_{DMM} - x_W) + C(x_{DMM} - x_W)^2] \quad (13)$$

Subsequently, a smooth curve of ΔG^{mix} ($=\Delta G^{excess} + \Delta G^{ideal}$) can be obtained. From the ΔG^{mix} curve the position of the phase boundaries were determined by using the double tangent method [21,22]. This method is based on the fact that the free energy curves of partially miscible binary mixture has concave parts with points associated with a negative curvature, which can be used to find two points on the curve that share the same tangent, which means the chemical potentials of both components at these compositions are exactly the same.

For validation of the force field, we also calculated heat of vaporization and surface tension. The heat of vaporization, ΔH_{vap}, was calculated using the following equation.

$$\Delta H_{vap} = E_{intra}(g) - (E_{intra}(l) + E_{inter}(l)) + RT \quad (14)$$

The assumption is that the vapor phase obeys ideal gas law. $E_{intra}(g)$ was obtained by ensemble average of the gas-phase simulation, $E_{intra}(l)$ is intramolecular energy and $E_{inter}(l)$ is intermolecular energy, both in the liquid phase. The surface tension was calculated by applying Kirkwood–Buff formula originally developed by Tolman [23] and refined by Kirkwood and Buff [24]. The surface tension is calculated as an integral of the difference between the normal and tangential pressure P_N and P_T: [25]

$$\gamma_P = \frac{1}{2}\int_{-\infty}^{\infty}(P_N(z) - P_T(z))dz \quad (15)$$

where z is along the direction normal to the interface, $P_N(z) = P_z(z)$ and $P_T(z) = (P_x(z) + P_y(z))/2$. The integrand is a function of z coordinate; it is zero at bulk (vacuum and liquid) phases and non-zero at the interfacial regions. Considering the integrand as a distribution function, the integral can be replaced with an ensemble average over time and z-dimension:

$$\gamma_P = \frac{L_z}{2}\left\langle P_N - P_T \right\rangle \quad (16)$$

Table 2
Calculated properties of DMM with OPLS force field.

	T (K)	Cal.	Exp.	Dev (%)
Density (g/cm^3)	298	0.909 (2)	0.899	1
	448	0.731 (1)		
H_{vap} (kJ/mol)	448	44.11	41.69	6
Surface tension (mN/m)	298	27 (3)	26.3	3

The outer factor of 1/2 in Eq. (16) accounts for the presence of two liquid–vapor interfaces which is commonly used in modeling the liquid–vapor interface.

The simulation procedure is summarized as follows. First, energy minimization was performed to relax the prepared simulation box with a maximum of 1000 steps. Then the simulation box was equilibrated for 1 ns. Finally the data collection was run for 2 ns. Each of the simulation procedure took about 12 CPU hours on a 2.5 GHz single processor. We calculated 2 pure liquids and 10 mixtures at 4 different temperatures. For each of the systems, chemical potentials were evaluated using 26 λ-point TI simulations. Therefore, 2288 simulations were carried out to finish one set of data, which required approximately 9 CPU days on a 128-processor computer. In order to estimate uncertainties in the calculated ΔG^{mix}, we generated 2–3 independent sets of data.

3. Results and discussion

3.1. Validation of force fields

Density, heat of vaporization (H_v) and surface tension of pure DMM were calculated using the OPLS all-atom force field at two temperatures. The computational and experimental data are listed in Table 2 for comparison. At 298 K, the calculated density and surface tension are in excellent agreement with the experimental data with 1% and 3% deviations respectively. The heat of vaporization calculated at the boiling point (448 K) is 6% greater than the experimental data, which is a typical result for a general force field. These results demonstrate that the OPLS all-atom force field is capable for describing physical properties of pure DMM.

In order to validate the force field for mixtures, we calculated the hydration free energies (ΔG_{hyd}) for dimethyl ether and diethyl ether. The simulation results are shown in Table 3. It is clear that the hydration free energies are underestimated by about 60% for both molecules, which is consistent with the data reported by Mobley et al. [26] who compared computational and experimental data for much larger data set (504 neutral small organic molecules) using the AMBER force field [27] and TIP3P water [28] and found systemic underestimates in the calculated hydration energies.

These underestimates are originated from the fact that a classical force field fails to represent the polarization effect, which leads to underestimate the interactions between ether and water molecules. In addition, we noticed incorrect phase separation of DMM and water mixture using the OPLS force field, which is consistent with the underestimate. One answer to this problem would be polarizable force field [8]. However, since the underestimate is systematical, and the polarization is due to the same solvent (water), we chose to introduce an average modification

Table 3
Comparison of calculated ΔG_{hyd} (kJ/mol) of dimethyl ether and diethyl ether with OPLS and modified OPLS force field (OPLS+[a]) and experimental results.

	OPLS	OPLS+	Exp.
Dimethyl ether	2.96 (1)	7.47 (7)	7.99
Diethyl ether	2.4 (3)	6.97 (5)	6.65

[a] A scaling factor of 0.95 is applied to geometrically combined VDW δ_{ij} parameters for atom pairs from different molecules.

Table 4
The ΔG of DMM and water in different compositions.

n (mol%)	DMM (kJ/mol)				Water (kJ/mol)			
	283 K	323 K	333 K	353 K	283 K	323 K	333 K	353 K
0	–	–	–	–	−26.5 (0.1)	−24.77 (0.6)	−24.2 (0.1)	−23.3 (0.1)
1	−34.4 (0.8)	−26.5 (0.8)	−24.2 (1.0)	−23.0 (0.4)	−26.6 (0.1)	−24.5 (0.1)	−24.1 (0.3)	−23.0 (0.2)
6	−37.2 (0.4)	−31.2 (0.7)	−29.4 (2.0)	−26.1 (0.4)	−26.4 (0.6)	−23.91 (0.1)	−23.5 (0.2)	−22.3 (0.1)
20	−37.8 (2.9)	−32.3 (0.4)	−30.0 (1.0)	−28.3 (0.2)	−24.3 (0.2)	−22.0 (0.2)	−21.14 (0.1)	−20.0 (0.2)
31	−36.6 (1.0)	−30.7 (0.6)	−30.9 (0.8)	−28.8 (0.8)	−24.6 (0.2)	−21.3 (0.3)	−19.3 (1.1)	−18.8 (0.2)
40	−34.8 (2.3)	−30.0 (0.7)	−29.5 (1.2)	−27.0 (0.1)	−23.1 (0.4)	−20.5 (0.3)	−19.4 (0.1)	−18.3 (0.1)
50	−32.6 (1.6)	−29.1 (0.3)	−27.3 (1.9)	−26.6 (0.3)	−23.9 (0.5)	−20.0 (0.3)	−19.2 (0.6)	−17.4 (0.3)
60	−31.9 (0.2)	−28.5 (0.9)	−26.8 (0.6)	−27.0 (0.1)	−23.1 (0.7)	−19.7 (0.3)	−18.97 (0.1)	−16.6 (0.2)
68	−33.6 (0.4)	−28.2 (0.5)	−26.6 (0.6)	−26.3 (0.1)	−23.9 (0.4)	−19.6 (0.5)	−18.6 (0.1)	−16.8 (0.4)
84	−31.8 (0.1)	−28.0 (1.5)	−26.7 (0.2)	−25.4 (0.5)	−22.6 (0.1)	−18.5 (0.4)	−17.8 (0.3)	−15.9 (0.1)
90	–	−27.5 (0.6)	−26.5 (0.6)	–	–	−18.3 (0.8)	−17.0 (0.2)	–
100	−32.3 (1.0)	−27.7 (0.4)	−26.3 (0.4)	−25.5 (0.44)	–	–	–	–

to effectively represent the polarization. After examination of a couple of options, we modified the combined vdW radius between atoms of ethers and water by scaling the geometric combining rule ($\sqrt{\delta_{ii}\delta_{jj}}$) by 0.95. Table 3 showed the ΔG_{hyd} calculation results of dimethyl ether and diethyl ether with this effective force field which is referred as OPLS+ in this paper. The modification significantly improved the prediction. The deviations in calculate hydration free energies of both ethers are within 7%, and the incorrect phase separation is eliminated using the modified force field. The OPLS+ force field was used in the computation of free energies of DMM aqueous solution.

3.2. Computation of Gibbs free energy of mixing

Fig. 3 shows the representative $\langle dV/d\lambda \rangle$ curves calculated for decoupling one DMM from liquid DMM and one water from liquid water using the selected λ values. The $\langle dV/d\lambda \rangle$ curves obtained by three independent simulations and the averaged curve are shown in Fig. 3. The standard deviations estimated from three independent samples are ca. 0.3 kJ/mol for both cases. As commonly seen in the TI calculations, the calculated $\langle dV/d\lambda \rangle$ curves bear sharp changes as the λ value varies. However, the curves are generally smooth enough for numerical integration. In addition, the $\langle dV/d\lambda \rangle$ values obtained are within a relatively small range of 150 kJ/mol, which effectively limits the uncertainty of the integration.

Table 4 shows the calculated ΔG of DMM and Water in a range of selected compositions. The precision of the predictions is reasonably high as shown by the uncertainties given in the parenthesis. The average standard deviations are 0.8 kJ/mol for DMM and 0.3 kJ/mol for water.

The free energies were calculated for mixtures in which the binary molecules were fully mixed. Some of the configurations are high in free energies and they do not exist in real life. The free energies of the "virtual" configurations can be estimated if the simulation models are stable during the simulation period. We tested the stability of the simulation models. As shown in Fig. 4, the radial distribution functions (RDF) of DMM–DMM, DMM–water and water–water for the 20 mol% mixture at 353 K are almost identical before and after the TI process. It should be noted that this model represents one of those most unstable configurations as shown later in this paper (see Fig. 8).

The *PV* contribution to the calculated free energy difference is minimal. Fig. 5 shows the volume changes as one DMM is decoupled from the liquid DMM. The total volume decreases 0.3 nm^3, which is roughly equivalent to the molecular volume of DMM. Under one atmosphere this volume change would contribute to ca. 0.02 kJ/mol to the free energy. Consider the cancelation between ΔG^{sol} and ΔG^{pure} the *PV* contribution to ΔG^{mix} is even smaller. Therefore, we did not include PV contributions to the free energies in this work.

The excess molar volumes (V_m^E) at different molar fractions and temperatures are displayed in Fig. 6. It is of interest to note that negative values are observed, which is similar to the trend of other ether–water mixtures [29,30].

The calculated ΔG^{excess} data were used to fit the Redlich–Kister equation (Eq. (13)). Fig. 7 shows the fitted ΔG^{excess} curves as functions of DMM molar percent (mol%). The fit quality measured by coefficients of determination (R-square) as given in Table 5 is excellent for data obtained at 323 K, reasonably good for data of 333 K and 353 K, but very poor at 283 K. A comparison of dipole autocorrelation functions (ACT) of a sample at 283 K and a sample

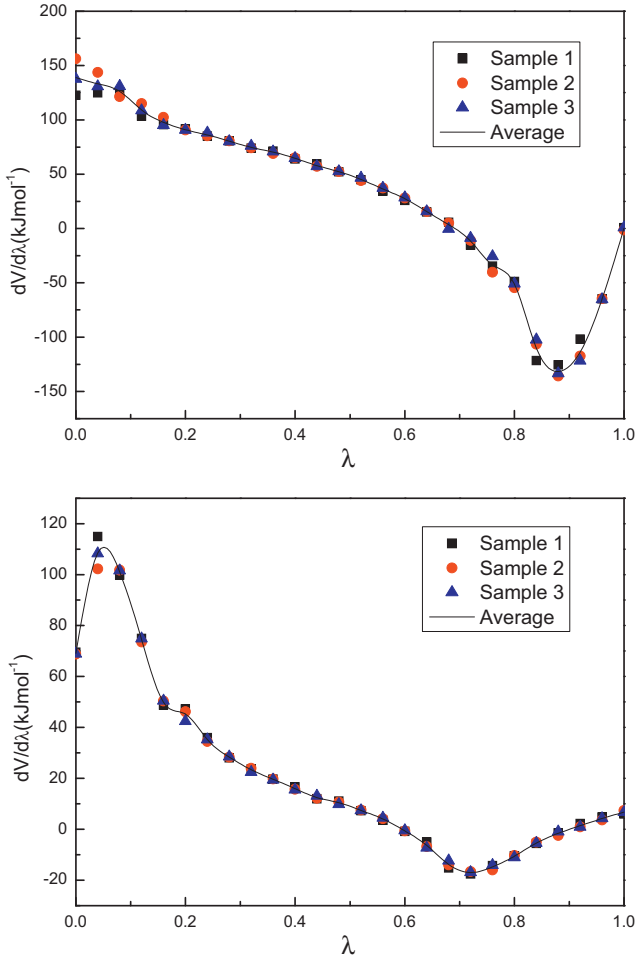

Fig. 3. The $\langle dV/d\lambda \rangle$ curves calculated for decoupling one DMM from liquid DMM (top) and one water from liquid water using a series of λ values (bottom).

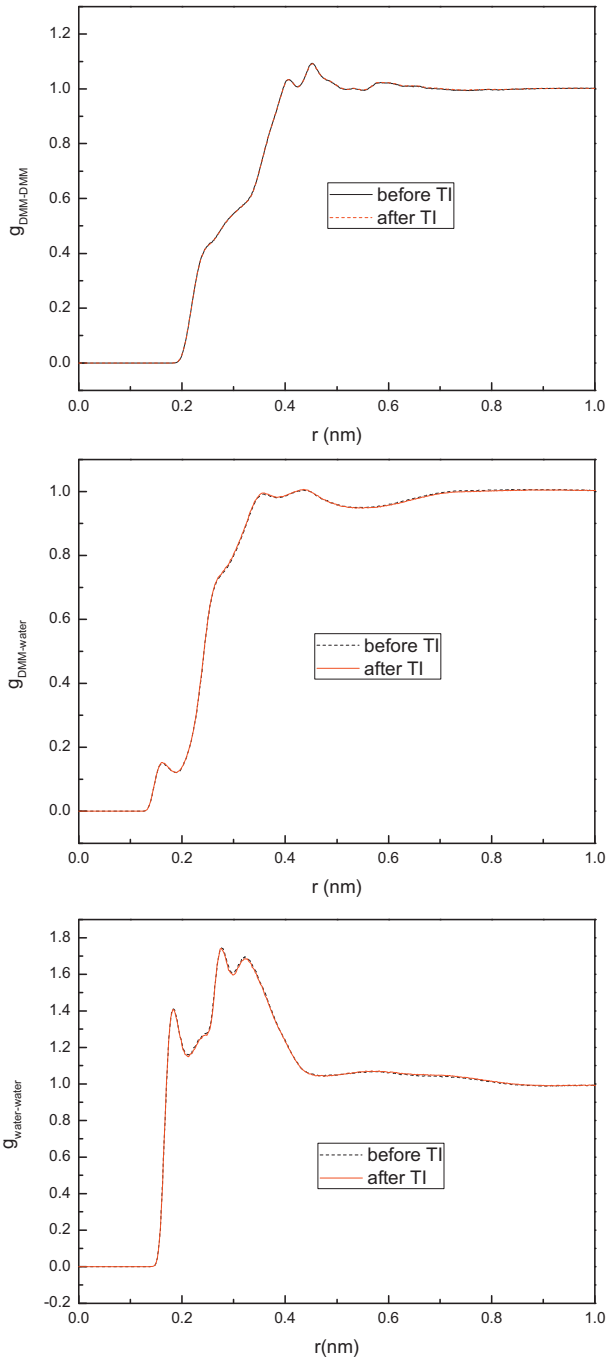

Fig. 4. Radial distribution functions $g(r)$ of DMM–DMM, DMM–water and water–water before TI (black solid line) and after TI (red dash line) at 353 K with DMM mol concentration 20%. (For interpretation of the references to color in this figure legend, the reader is referred to the web version of the article.)

at 353 K indicated that the correlation time of the 283 K sample is roughly three times longer than that of the 353 K sample. Therefore, the large uncertainty observed at 283 K is likely related to insufficient samplings. At 353 K the average standard deviation of DMM free energy calculation is only 0.33 kJ/mol, but it is as large as 1.07 kJ/mol at 283 K. The correspond ΔG^{ideal} which can be calculated analytically are also displayed in the figure.

The estimated standard errors on the C parameter given in Table 5 indicate that this parameter is probably not significant. Using only two parameters (A and B) similar fit quality was obtained using the same data given in Table 4. However, parameter C in the Redlich–Kister equation is important for the shape of the ΔG^{excess} curve as it introduces a higher-order term in the equation. The curves obtained using two parameters are quite different in shape from those obtained using three parameters. Attempt to predict mutual solubility using the 2-parameter Redlich–Kister equation lead to much worse prediction.

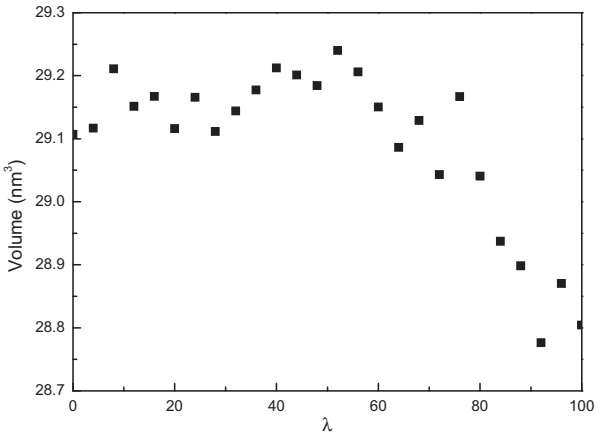

Fig. 5. Volume change during decoupling one DMM from liquid DMM.

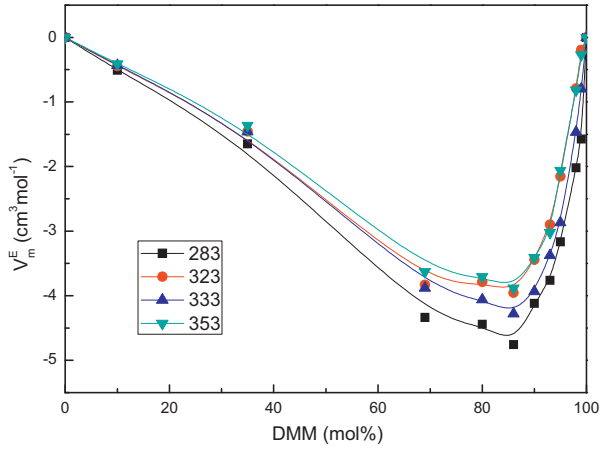

Fig. 6. Excess molar volume (V_m^E) for DMM + water at 283 K (square), 323 K (circle), 333 K (up triangle) and 353 K (down triangle).

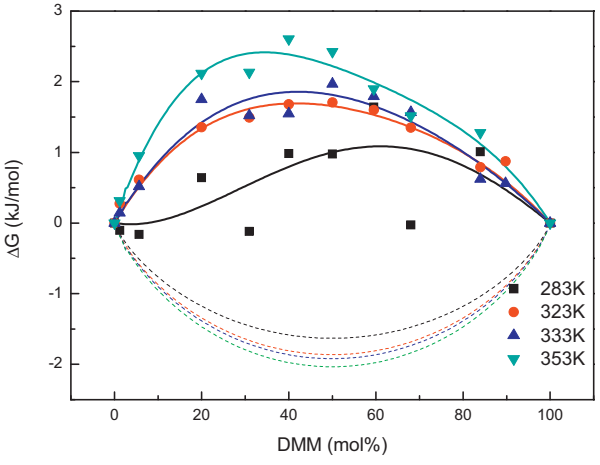

Fig. 7. ΔG^{excess} of DMM and water mixtures as a function of the mol% concentration (DMM) at 283 K (square), 323 K (circle), 333 K (up triangle) and 353 K (down triangle). Calculated ΔG^{excess} of DMM were fitting to Redlich–Kister equation, shown as solid lines. ΔG^{ideal} is also shown as dot line.

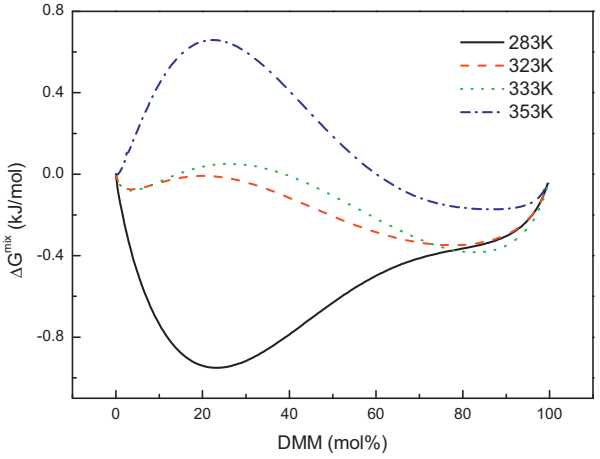

Fig. 8. ΔG^{mix} of DMM and water mixtures as a function of the mol% concentration (DMM) at 283 K (black solid line), 323 K (red dash line), 333 K (green dot line) and 353 K (blue dash dot line). (For interpretation of the references to color in this figure legend, the reader is referred to the web version of the article.)

Fig. 8 shows the ΔG^{mix} curves which are combinations of ΔG^{excess} and ΔG^{ideal} as functions of molar concentrations of DMM at investigated temperatures. Two upward curvatures (UC), a typical pattern of partial miscible binary mixture, can be observed for the curves of 283, 323 and 333 K. At 283 K, the first UC is broad and deep with the minimum located at around 22 mol%. The second UC is very shallow and short. The ΔG^{mix} curves obtained at 323 K and 333 K show two UCs. The first is relatively shallow and short, ranging from 0 to 20 mol%; the second UC is much deeper and broader, with the minimum at approximately 96 mol%. A comparison of these two curves shows that the first minima are nearly the same and the second shifts to higher concentration as the temperature increases from 323 to 333 K. The ΔG^{mix} curve of 353 K is mostly above zero, indicating the mixture is unstable. A close examination shows that there are two UCs in the curve. One is around 80 mol%, and another is very close to 0 mol%.

Using the double tangent method, we predict the mutual solubility at different temperatures. ΔG^{mix} is expressed in analytical term using the Redlich–Kister equation. The double tangents were solved using SciPy [31] an open-source software for scientific computation. These results are summarized in Table 6.

Table 5
The coefficients of the Redlich–Kister equation fit to the excess Gibbs free energies.

T (K)	A	B	C	R-square
283	1.5 (0.5)	−1.1 (1.2)	−0.7 (2.7)	0.25
323	2.5 (0.1)	0.7 (0.2)	0.7 (0.4)	0.97
333	2.6 (2)	0.8 (0.4)	0.3 (0.8)	0.93
353	3.0 (0.1)	1.5 (0.3)	1.7 (0.8)	0.96

Table 6
The predicted mutual solubility (mol% DMM) at 283 K, 323 K, 333 K and 353 K. The deviations of the calculated results were list in parenthesis.

T (K)	Upper phase		Lower phase	
	Cal.	Exp.	Cal.	Exp.
283	0.86 (4)	0.36	0.4 (1)	0.078
323	0.70 (1)	0.69	0.03 (1)	0.026
333	0.78 (2)	0.68	0.03 (2)	0.021
353	0.79 (8)	0.68	0.002 (2)	0.015

4. Conclusions

By scaling the combining rule of VDW radius, the polarization between unlike molecules can be effectively introduced, judging by predictions of hydration free energies of ethers.

Free energies were calculated at various compositions based on fully-mixed binary models or pure substance models. The mixture models were stable during the TI simulation period (8 ns) which provides the possibility to estimate the free energies for the entire composition range and to deduce the mutual solubility from the free energy curves. The ΔG data were predicted at fairly high precision level using the TI method and current computational resource. The average uncertainties in calculated ΔG^{excess} are 0.8 kJ/mol for DMM and 0.3 kJ/mol for water. However, the uncertainties are still too large to predict the mutual solubility accurately. Nevertheless, by fitting the calculated ΔG^{mix} curves to an analytical form and solving the double tangents mathematically, the solubility data obtained appear to be reasonable. In principle, the quality of prediction can be improved with increasing computational power.

Acknowledgements

We acknowledge Dr. Xiaofeng Li and Dr. Lifeng Zhao for beneficial discussions. Also, we acknowledge Shanghai Supercomputer Center (SSC) and the High Performance Computing Center (HPCC) of Jilin University for the computing time. This work was partially funded by National Science Foundation of China NSAF Program (No. 10676021) and National Basic Research Program of China (No. 2007CB209701).

References

[1] A.Z. Panagiotopoulos, Mol. Phys. 61 (1987) 813–826.
[2] T.I. Morrow, E.J. Maginn, J. Chem. Phys. 122 (2005) 054504.
[3] J.J. Potoff, A.Z. Panagiotopoulos, J. Chem. Phys. 109 (1998) 10914–10920.
[4] M.H. Lamm, C.K. Hall, Fluid Phase Equilib. 194–197 (2002) 197–206.
[5] A. Lotfi, J. Vrabec, J. Fischer, Mol. Phys. 76 (1992) 1319–1333.
[6] T. Kristóf, J. Liszi, D. Boda, Mol. Phys. 100 (2002) 3429–3441.
[7] J. Dai, X. Li, L. Zhao, H. Sun, Fluid Phase Equilib. 289 (2010) 156–165.
[8] J.W. Ponder, C. Wu, P. Ren, V.S. Pande, J.D. Chodera, M.J. Schnieders, I. Haque, D.L. Mobley, D.S. Lambrecht, R.A. DiStasio, M. Head-Gordon, G.N.I. Clark, M.E. Johnson, T. Head-Gordon, J. Phys. Chem. B 114 (2010) 2549–2564.
[9] T. Schnabel, J. Vrabec, H. Hasse, J. Mol. Liq. 135 (2007) 170–178.
[10] H.J.C. Berendsen, J.R. Grigera, T.P. Straatsma, J. Phys. Chem. 91 (1987) 6269–6271.
[11] W.L. Jorgensen, D.S. Maxwell, J. Tirado-Rives, J. Am. Chem. Soc. 118 (1996) 11225–11236.
[12] B. Hess, C. Kutzner, D. van der Spoel, E. Lindahl, J. Chem. Theory Comput. 4 (2008) 435–447.
[13] G. Bussi, D. Donadio, M. Parrinello, J. Chem. Phys. 126 (2007) 014101.
[14] M. Parrinello, A. Rahman, J. Appl. Phys. 52 (1981) 7182–7190.
[15] B. Hess, H. Bekker, H. Berendsen, J. Fraaije, J. Comput. Chem. 18 (1997) 1463–1472.
[16] D. Tom, Y. Darrin, P. Lee, J. Chem. Phys. 98 (1993) 10089–10092.
[17] M.R. Darvas, P.L. Jedlovszky, G.B. Jancsoï, J. Phys. Chem. B 113 (2009) 7615–7620.
[18] B.C. Stephenson, K.A. Stafford, K.J. Beers, D. Blankschtein, J. Phys. Chem. B 112 (2008) 1641–1656.
[19] T.C. Beutler, A.E. Mark, R.C. van Schaik, P.R. Gerber, W.F. van Gunsteren, Chem. Phys. Lett. 222 (1994) 529–539.
[20] P. Sabarathinam, Ind. Eng. Chem. Res. 33 (1994) 752.
[21] J. Huang, G.W. Feigenson, Biophys. J. 65 (1993) 1788–1794.
[22] A. Liu, T.L. Beck, J. Chem. Phys. 105 (1996) 2424–2428.
[23] R.C. Tolman, J. Chem. Phys. 16 (1948) 758–774.
[24] J.G. Kirkwood, F.P. Buff, J. Chem. Phys. 17 (1949) 338–343.
[25] A.E. Ismail, M. Tsige, P.J.V. In, G.S. Grest, Mol. Phys. 105 (2007) 3155–3163.
[26] D.L. Mobley, C.I. Bayly, M.D. Cooper, M.R. Shirts, K.A. Dill, J. Chem. Theory Comput. 5 (2009) 350–358.
[27] J. Wang, R.M. Wolf, J.W. Caldwell, P.A. Kollman, D.A. Case, J. Comput. Chem. 25 (2004) 1157–1174.
[28] W.L. Jorgensen, J. Chandrasekhar, J.D. Madura, R.W. Impey, M.L. Klein, J. Chem. Phys. 79 (1983) 926–935.
[29] A. Pal, Y.P. Singh, J. Chem. Eng. Data 41 (1996) 425–427.
[30] A. Pal, G. Dass, A. Kumar, J. Chem. Eng. Data 43 (1998) 738–741.
[31] SciPy, http://www.scipy.org/.